EPiC Series in Engineering
Volume 5, 2023, Pages 104–113
Proceedings of International Symposium on Applied Science 2022

Analysis of the impact of near-infrared light on the skin surface to the cervical vertebrae

Nguyen Huu Nhat Thong[1,2] and Trinh Tran Hong Duyen[1,2]
[1] Department of the Biomedical Engineering, Faculty of Applied Science, Ho Chi Minh City University of Technology (HCMUT), 286 Ly Thuong Kiet Street, District 10, Ho Chi Minh City, Vietnam
[2] Vietnam National University Ho Chi Minh City, Linh Trung Ward, Thu Duc District, Ho Chi Minh City, Vietnam
thong.nguyenaka@hcmut.edu.vn, tt_hd2005@hcmut.edu.vn

Abstract

In the musculoskeletal system, the spine determines the life and movement of humans as well as that of all other vertebrates. The degenerative spine usually begins with damaged joints of the vertebral bodies, neck herniated disc, ligament, and then gradually occurs degeneration of the vertebrae, causing neck pain, especially when moving the neck area.

Nowadays, along with the development of the biomedical field, low-power laser therapy is more prominent in its applicability in diagnosis and treatment. This paper describes the simulation results of low-level laser propagation from the skin surface to the cervical vertebrae with four wavelengths (633 nm, 780 nm, 850 nm, and 940 nm) by the Monte Carlo method. These simulation results are the base for analyzing the impact of near-infrared light and developing a low-level laser therapy device, that could be used clinically for treating the degenerative spine.

Author keys: Monte Carlo simulation; low-level laser therapy LLLT; cervical vertebrae; degenerative spine.

1 Introduction

The term "cervical spondylosis" refers to a variety of gradually developing degenerative alterations that affect every part of the cervical spine (i.e., intervertebral discs, facet joints, joints of the Luschka, the ligamenta flava, and the laminae). The majority of people begin to experience it after their fifth decade of life, and it is a natural part of aging. When neural structures are compressed, cervical spondylosis symptoms such as neck pain and stiffness may be accompanied by radicular symptoms [2]. The majority of adults with spondylotic alterations of the cervical spine on

radiographic imaging are asymptomatic, with degenerative changes being evident in 25% of people under the age of 40, 50% of people over the age of 40, and 85% of those over the age of 60. C6-C7 and C5-C6 are the levels that are most commonly impacted. The most typical symptom of symptomatic cervical spondylosis is neck pain. The point prevalence of neck discomfort in the general population ranges from 0.4% to 41.5%, 1-year incidence from 4.8% to 79.5%, and lifetime prevalence up to 86.8% [3].

Low-Level Laser Therapy (LLLT) is an application developed and applied widespread in the field of medicine in today's world which stimulates tissue regeneration, relieves pain and inflammation. Unlike any other medical laser applications, the LLLT does not have mechanism of ablation or thermal, but a photochemical effect meaning light is absorbed resulting in photochemical reaction inside the biological tissues.

This paper depicts the model construction and the propagation of the low-level laser from the skin surface layer to the cervical vertebrae layer through the Monte Carlo method. This Monte Carlo-based simulation mimics the light propagation inside the multi-layered tissue, the anatomical structure in the human body, and the optical parameters of the biological tissues. The results show that the power density ranging from ($1.0 - 10^{-4}$ W/cm^2) of the specific wavelengths (633 nm, 780 nm, 850 nm, and 940 nm) which exhibit the "effective operating area" of the low-level laser beam on the tissue being treated. The fact ultimately states that the choice of wavelength, power density, and appropriate dosage affect the treatment process.

2 Materials and Methods

2.1 Monte Carlo method

The Monte Carlo method is the main technique used to describe the simulation of light transmission in biological tissues in this paper [4]. The mentioned method is applied to simulate the propagation of light in biological tissues based on the Radiative transport equation (RTE) and simulated calculations, calculating the propagation of photons in the absorption and scattering medium [5-11]. The radiative transport equation (RTE) is a popular equation for describing particle propagation in the complex structure of tissues [5].

A photon is a unit of light. The wave properties of a photon are ignored in this paper, it only deals with the properties of the particle. Therefore, the phase and polarization parameters of the light are not taken into account. In the simple case, the photon is introduced into an independent medium and its motion is recorded until it is absorbed or scattered out of the field of view. Although the results are highly accurate, this method demands repeated computations to achieve the desired accuracy, resulting in the simulation implementation being time consuming. For example, to achieve 0.1% accuracy, the movement of 1000000 photons must be performed.

A Monte Carlo simulating method described by Prahl [6] and programmed by Wang and Jacques [7] employs the technique of capturing the hidden photon called "existing weights". Photons have their "initial weight" and will decrease with each move until scattered without a stop for each photon in the scattering process until they are finished by an absorption one. By that, the statistics would be more effective and efficient skipping the computational process of the movement of the photons which takes plethora steps until the end in the absorption process.

2.2 Simulation models

The structure from the skin surface to the cervical vertebrae is classified into 4 layers: human skin ~ 0.3 cm, subcutaneous fat ~ 1.0 cm, musculus trapezius ~ 2.0 cm; and cervical vertebrae ~ 2.0 cm.

Human skin consists of stratum-cormeum, epidermis, demis with the thickness approximately (0.06 – 0.1 cm), (0.0006 – 0.015 cm), (0.06 – 0.3 cm) [14-16]. In this paper, we focus on the model with a thickness of 0.3 cm.

The aborted coefficient μ_a and the scattered coefficient μ_s are the probability density functions whose reciprocals can be interpreted as the average mean distances for the absorption and scattering. The sum of them is called the total attenuation characterizing the reaction of the photon's mean per unit of path length. Anisotropy coefficient g is the value of the cosine of angle average deviation scattering θ of the angle between the direction of the photons being scattered and incident photons, characterizes the isotropy of the medium. These aforementioned parameters characterize the properties of the tissue layers and are published internationally with credibility which is present in Table 1.

Table 1: The optical parameters of the tissues

Tissue	λ (nm)	n	μ_a (cm^{-1})	μ_s (cm^{-1})	g
Skin [17-19]	633	1.4	0.334	272.9	0.9
	780		0.142	197.3	0.9
	850		0.1223	175.73	0.9
	940		0.1905	156.7	0.9
Subcutaneous fat [8]	633	1.44	0.128	125.5	0.91
	780		0.0846	114.67	0.91
	850		0.086	110.9	0.91
	940		0.168	108.6	0.91
Musculus trapezius [8]	633	1.37	1.32	89.6	0.93
	780		0.331	71.2	0.93
	850		0.295	66.0	0.93
	940		0.401	58.1	0.93
Cervical vertebrae [8]	633	1.4	0.122	106.66	0.85
	780		0.073	88	0.85
	850		0.092	82	0.85
	940		0.172	79.33	0.85

The simulated result is performed under the precision value of 0.1% being calculated with 1000000 photons based on the Monte Carlo Multi-Layered (MCLC) program [7] in unison with its companion called CONV [9] to optimize the performance and reduce the simulation. Laser power would change complying with the required position for the desired results continuously, with the Gaussian-shaped spatial beam profile (radius $1/e^2$ is 0.14 cm). The simulated results display the distribution of power density of 10^{-4} W/cm^2 at which laser beam can cause biological effects on the tissue stimulation.

3 Results

3.1 MCML program

We measure the light density distribution along the horizontal axis by using the 1 cm intervals for the reflective and transmitted edges. The MCML program would be executed under the file named "file.mci" inputting the data prepared, when the calculation is finished, the output result would be performed under the "file.mco" using the MATLAB machine language which is usually used to

launch the ".m" files. These simulation results show the distribution of power density of 10^{-4} W/cm^2 - at which the laser beam causes the stimulation biological effect on tissue. The output file of MCML is handled by the program named "conv.exe" to respond to an infinite photon beam and to compute the finite size beams of photon. Initial beams mostly propagate along the vertical axis then gradually disperse over different directions. After the program being invoked, the menu system will direct the data input, output, or process – "file.iso". We used Excel software to produce publication-quality graphs and fit data with arbitrary curves.

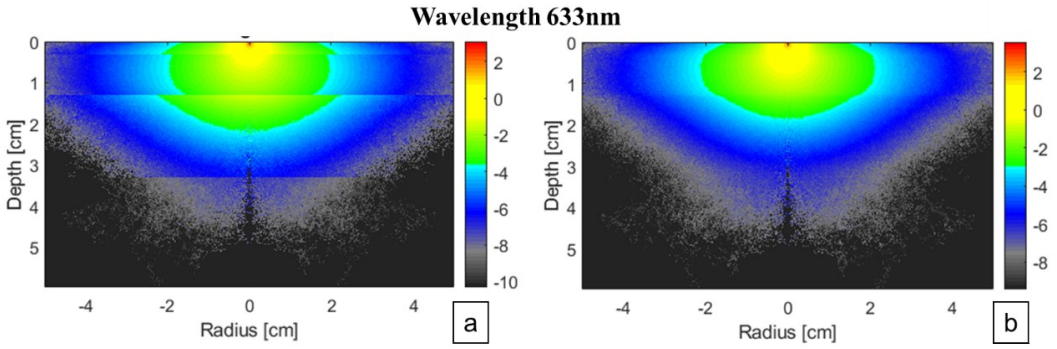

Figure 1: Absorbed energy distribution and incident flux distribution at 633 nm

Figure 1 describe the absorbed energy density distribution and the photon flux distribution at 633 nm according to the depth z (cm) and radius r (cm) from the MCML program. The light source is defined as the point of the laser beam at □ = 0, z = 0 at the neck skin surface. Regarding the power density distribution, the MCML program results in the absorbed energy density per unit of time. The power density distribution is plotted in log form representing the color scale. The discontinuity at the intervals between tissue layers is due to differences in absorption coefficients owing to the occurrence of non-absorption scattering at the boundary. During the propagation of photons from the skin surface to the cervical vertebrae at 633 nm, there is a $10^0 - 10^{-4}$ W/cm^2 power density photon deposition. Thus, photon propagation with absorbed power density of 10^{-4} W/cm^2 at 633 nm exists only in the dermal layer, subcutaneous fat layer, and muscle layer (reaching ~2.2 cm depth) and the largest radius of action in the muscle layer (~2.2 cm wide) – Figure 1a. Regarding the photon flux distribution, the flux distribution with a power density of 10^{-4} W/cm^2 for tissue layers has a continuum, the radius of effect gradually increases to a width of ~2.2 cm as the photon propagates from the surface. skin surface into adipose tissue. At a depth of approximately ~1.0 cm, the flux distribution with a power density of 10^{-4} W/cm^2 according to the radius of action does not continue to increase but gradually decreases and ends in the muscle layer – Figure 1b.

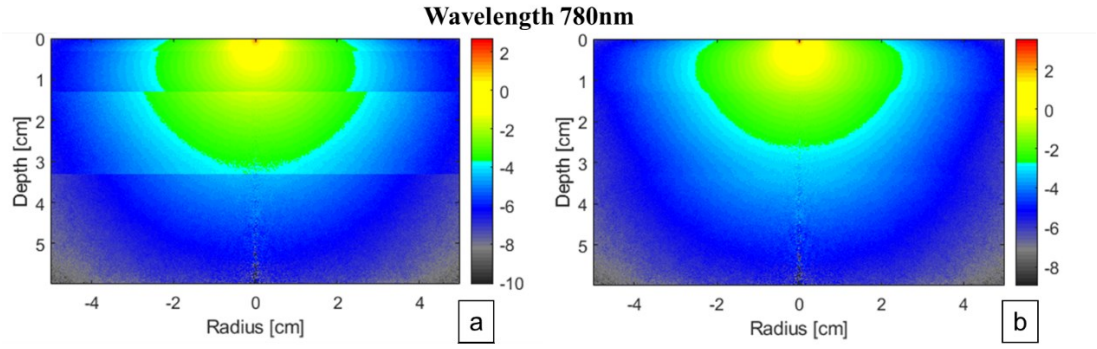

Figure 2: Absorbed energy distribution and incident flux distribution at 780 nm

Figure 2 describe the absorbed energy density distribution and the photon flux distribution at 780 nm according to the depth z (cm) and radius r (cm) from the MCML program. Regarding the power density distribution, the photon propagation with absorbed power density of 10^{-4} W/cm^2 at 780 nm exists only in the dermal layer, subcutaneous fat layer, and muscle layer (reaching ~3.2 cm depth) and the largest radius of action in the muscle layer (~2.7 cm wide) – Figure 2a. Regarding the photon flux distribution, the flux distribution with a power density of 10^{-4} W/cm^2 for tissue layers has a continuum, the radius of effect gradually increases to a width of ~2.5 cm as the photon propagates from the surface. skin surface into adipose tissue. At a depth of approximately ~1.4 cm, the flux distribution with a power density of 10^{-4} W/cm^2 according to the radius of action does not continue to increase but gradually decreases and ends in the muscle layer – Figure 2b.

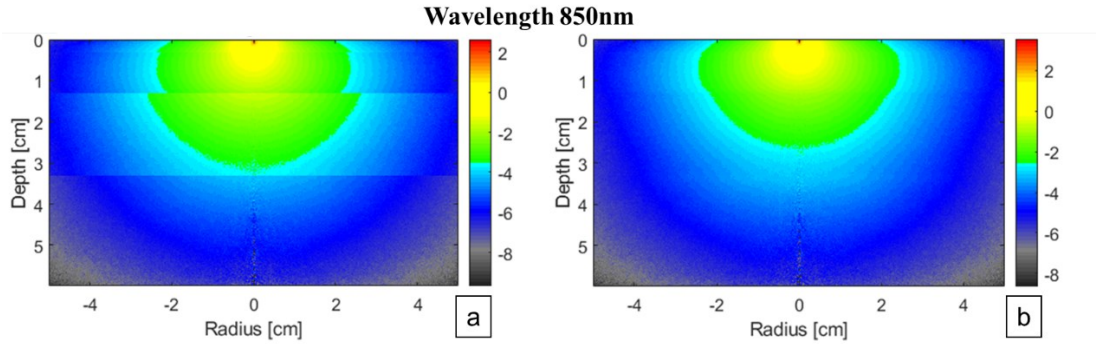

Figure 3: Absorbed energy distribution and incident flux distribution at 850 nm

Figure 3 describe the absorbed energy density distribution and the photon flux distribution at 850 nm according to the depth z (cm) and radius r (cm) from the MCML program. Regarding the power density distribution, the photon propagation with an absorbed power density of 10^{-4} W/cm^2 at 850 nm exists only in the dermal layer, subcutaneous fat layer, and muscle layer (reaching ~3.2 cm depth), and the largest radius of action in the muscle layer (~2.6 cm wide) – Figure 3a. Regarding the photon flux distribution, the flux distribution with a power density of 10^{-4} W/cm^2 for tissue layers has a continuum, the radius of effect gradually increases to a width of ~2.5 cm as the photon propagates from the surface. skin surface into adipose tissue. At a depth of approximately ~1.5 cm, the flux distribution with a power density of 10^{-4} W/cm^2 according to the radius of action does not continue to increase but gradually decreases and ends in the muscle layer – Figure 3b.

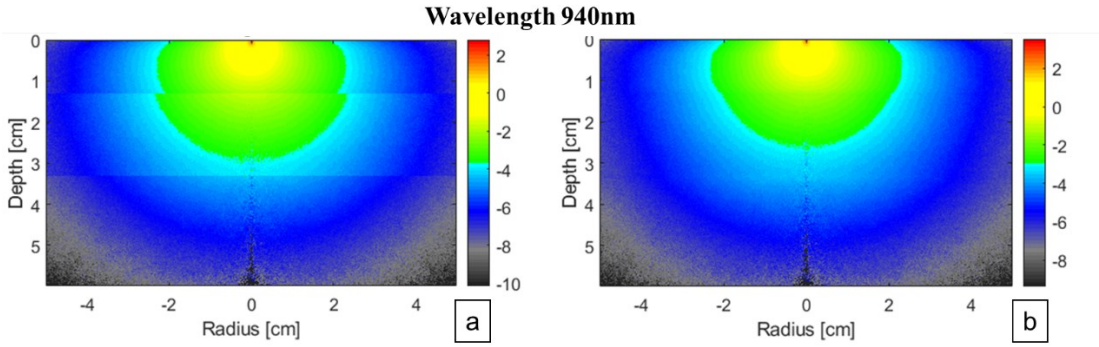

Figure 4: Absorbed energy distribution and incident flux distribution at 940 nm

Figure 4 describe the absorbed energy density distribution and the photon flux distribution at 940 nm according to the depth z (cm) and radius r (cm) from the MCML program. Regarding the power density distribution, the photon propagation with absorbed power density of 10^{-4} W/cm^2 at 940 nm exists only in the dermal layer, subcutaneous fat layer, and muscle layer (reaching ~3 cm depth) and the largest radius of action in the muscle layer (~2.4 cm wide) – Figure 4a. Regarding the photon flux distribution, the flux distribution with a power density of 10^{-4} W/cm^2 for tissue layers has a continuum, the radius of effect gradually increases to a width of ~2.4 cm as the photon propagates from the surface. skin surface into adipose tissue. At a depth of approximately ~1.0 cm, the flux distribution with a power density of 10^{-4} W/cm^2 according to the radius of action does not continue to increase but gradually decreases and ends in the muscle layer – Figure 4b.

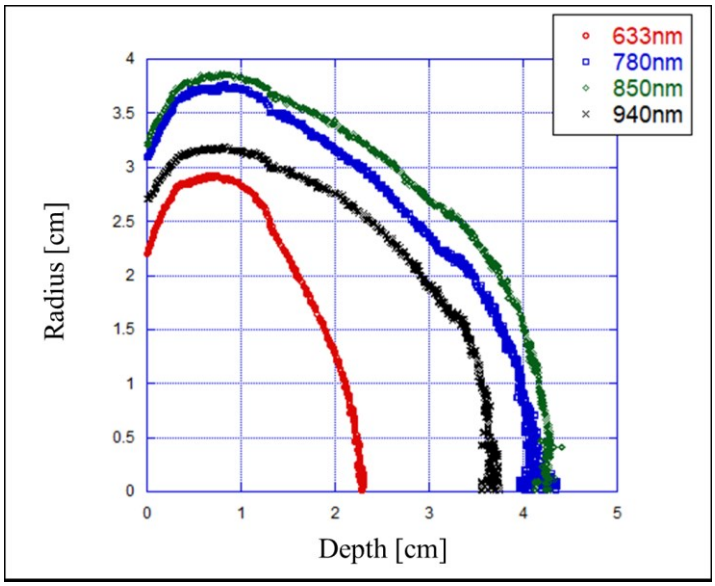

Figure 5: The penetrating ability of wavelengths (633 nm, 780 nm, 850 nm, and 940 nm) from the skin surface to cervical vertebrae at 10^{-4} W/cm^2 of power density

The simulation result is shown in Figure 5 from the skin's surface to the cervical vertebrae, using a 1J total energy for the Gaussian laser beam. In comparison to 940 nm (~3.7 cm), the penetration depth into tissue of 780 nm and 850 nm is relatively comparable (~4.2 cm). Less tissue may be penetrated

by the 633 nm wavelength (~2.3 cm). The "depth of penetration" and "impact radius" of the beam, on the other hand, both considerably rise as the irradiation period increases.

3.2 MOSE program

The model of layers from the skin to the cervical vertebrae is built based on the computed tomography image data set from the Carver College of Medicine, the University of Iowa (USA). Then use Materialize Mimics software to build 3D and mesh the model. The model is then fed into the MOSE program to simulate the propagation of photons in tissue from the skin surface to the cervical vertebrae [10, 11].

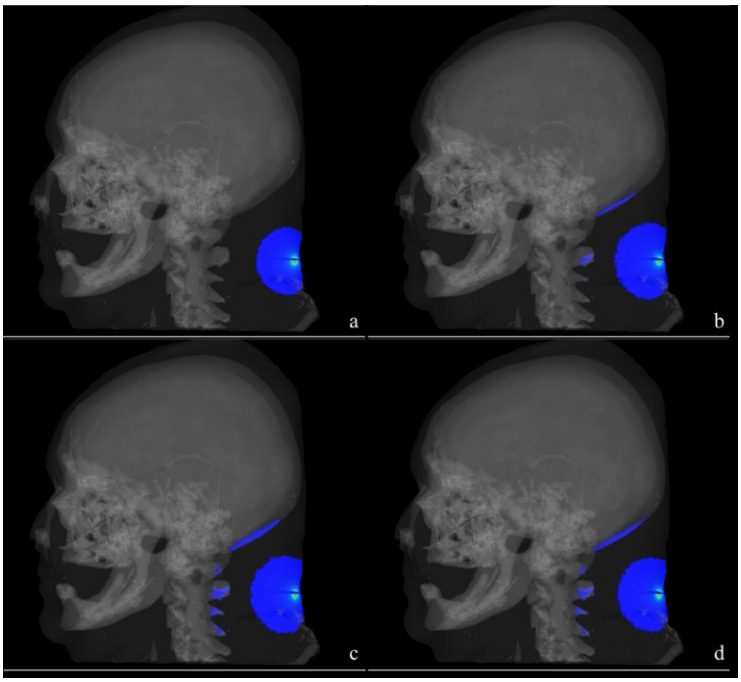

Figure 6: Absorption capacity with a total energy input of 1J from the MOSE program

Figure 6 depicts the results of absorption ability from the skin surface to the cervical vertebrae when irradiating a laser source with input energy of 1J from the MOSE program at four wavelengths of interest 633 nm, 780 nm, 850 nm, and 940 nm (in order a, b, c, d). At 633 nm, photon absorption only reaches the muscle layer surface and has not reached the cervical vertebrae surface. With the remaining three wavelengths, the photon absorption capacity reaches the surface of the cervical vertebrae. In which, the wavelength of 850 nm gives the best absorption results compared to the remaining wavelengths.

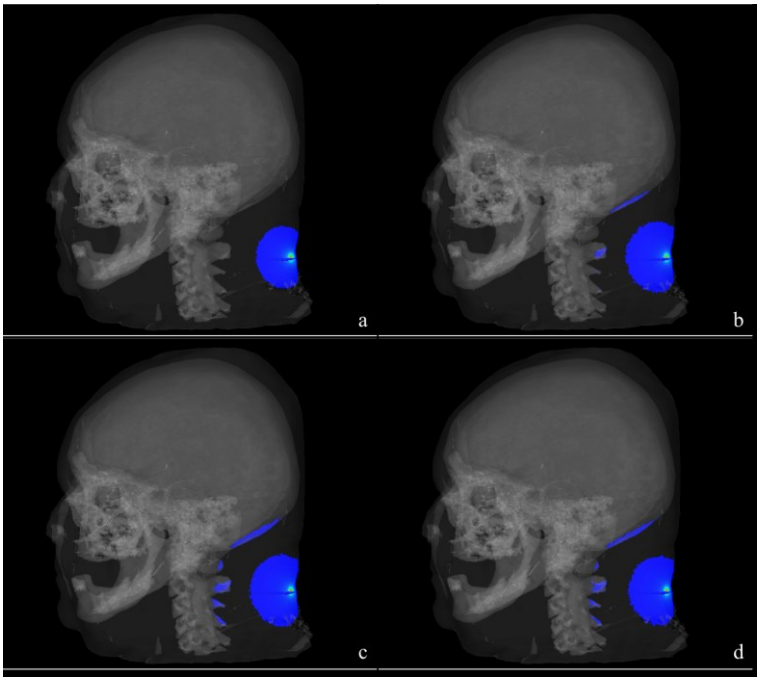

Figure 7: Absorption capacity with a total energy input of 4J from the MOSE program

Figure 7 depicts the results of absorption ability from the skin surface to the cervical vertebrae when irradiating a laser source with input energy of 4J from the MOSE program at four wavelengths of interest 633 nm, 780 nm, 850 nm, and 940 nm (in order a, b, c, d). At 633 nm, photon absorption only reaches the muscle layer surface and has not reached the cervical vertebrae surface. The photon absorption capacity reaches the cervical vertebral surface with the remaining three wavelengths and spreads to the occipital bone surface. In which, the wavelength of 850 nm gives the best absorption results compared to the remaining wavelengths.

The simulation results of the light propagation in the 3D model of the MOSE program are consistent with the results from the MCML program. From this result will help us to see an intuitive view of light propagation in the model of tissues with complex surfaces.

4 Conclusions

With the implementation of the low-level laser therapy (LLLT) and the use of the Monte Carlo method to simulate the propagation of the laser beam into the biological tissue, this paper state that the low-level laser of 780 nm, 850 nm, and 940 nm wavelength have significant impact to the tissue layers from the skin surface to the cervical vertebrae in which the 780nm and 850nm wavelength are the two best in the perspective of penetrating ability. The 2 mentioned ones are best suited to develop the LLLT devices. The irradiation time and the penetration depth and impact radius of the beams are directly proportional to each other, meaning that when the irradiation time increases, the "depth of penetration" and "impact radius" of the beam also increase.

Although out of the four, the 633 nm wavelength can reach the lowest depth compared to the other two, it can be used for skin treatment equipment or intravenous. The laser interacts with the component of blood, which improves microcirculation, balances the erythrocytes, and hemoglobin concentration, reduces the cholesterol, rheological properties, and blood lipids [12, 13]. Further

research and study can be executed by applying the low-level laser of 780 nm, 850 nm, and 940 nm wavelengths in the noninvasive LLLT from the skin surface in the treatment of degenerative spine.

Acknowledgments: This research is funded by Ho Chi Minh City University of Technology (HCMUT) - VNU-HCM.

References

[1] Á. Bernabéu-Sanz, J. V. Mollá-Torró, S. López-Celada, P. Moreno López and E. Fernández-Jover, "MRI evidence of brain atrophy, white matter damage, and functional adaptive changes in patients with cervical spondylosis and prolonged spinal cord compression," *European radiology,* vol. 30, no. 1, pp. 357-369, 2020.

[2] D. Shedid and E. C. Benzel, "Cervical spondylosis anatomy: Pathophysiology and biomechanics," *Neurosurgery,* vol. 60, no. 1, pp. S1-7, 2007.

[3] D. G. Hoy, M. Protani, R. De and R. Buchbinder, "The epidemiology of neck pain," *Best practice & research. Clinical rheumatology,* vol. 24, no. 6, pp. 783-792, 2010.

[4] N. Metropolis and S. Ulam, "The Monte Carlo method," *Journal of the American Statistical Association,* vol. 44, no. 247, pp. 335-341, 1949.

[5] S. Chandrasekhar, "Radiative transfer", London: Oxford University Press, 1950.

[6] S. Prahl, M. Keijze and S. Jacques, "A Monte Carlo Model of Light Propagation in Tissue," *SPIE,* vol. 5, 1989.

[7] L. Wang, S. L. Jacques and L. Zheng, "MCML-Monte Carlo modeling of light transport in multi-layered tissues," *Computer methods and programs in biomedicine,* vol. 47, no. 2, pp. 131-146, 1995.

[8] A. N. Bashkatov, E. A. Genina, V. I. Kochubey and V. V. Tuchin, "Optical properties of human skin, subcutaneous and mucous tissues in the wavelength range from 400 to 2000 nm," *Journal of Physics D: Applied Physics,* vol. 38, no. 15, pp. 2543-2555, 2005.

[9] L. Wang, S. L. Jacques and L. Zheng, "CONV - Convolution for responses to a finite diameter photon beam incident on multi-layered tissues," *Computer Methods and Programs in Biomedicine,* vol. 54, no. 3, pp. 141-150, 1997.

[10] S. Ren, X. Chen, H. Wang, X. Qu, G. Wang, J. Liang and J. Tian, "Molecular Optical Simulation Environment (MOSE): a platform for the simulation of light propagation in turbid media," *PloS one,* vol. 8, no. 4, p. e61304, 2013.

[11] H. Li, J. Tian, F. Zhu, W. Cong, L. V. Wang, E. A. Hoffman and G. Wang, "A mouse optical simulation environment (MOSE) to investigate bioluminescent phenomena in the living mouse with the Monte Carlo method," *Academic radiology,* vol. 11, no. 9, pp. 1029-1038, 2004.

[12] V. A. Mikhaylov, "The use of Intravenous Laser Blood Irradiation (ILBI) at 630-640 nm to prevent vascular diseases and to increase life expectancy," *Laser therapy,* vol. 24, no. 1, pp. 15-26, 2015.

[13] N. I. Nechipurenko, L. N. Anatskaia, L. I. Matusevich, I. D. Pashkovskaia and N. I. Shcherbina, "Effect of intravenous laser irradiation on some blood biochemical indicators in the acute stage of lacunar infarcts," *Zh Nevrol Psikhiatr Im S S Korsakova,* vol. 114, no. 7, pp. 43-48, 2014.

[14] S. T. Flock, B. C. Wilson and M. S. Patterson, "Monte Carlo modeling of light propagation

in highly scattering tissues. II. Comparison with measurements in phantoms," *IEEE transactions on bio-medical engineering,* vol. 36, no. 12, pp. 1169-1173, 1989.

[15] S. T. Flock, M. S. Patterson, B. C. Wilson and D. R. Wyman, "Monte Carlo modeling of light propagation in highly scattering tissues. I. Model predictions and comparison with diffusion theory," *IEEE transactions on bio-medical engineering,* vol. 36, no. 12, pp. 1162-1168, 1989.

[16] M. Keijzer, S. L. Jacques, S. A. Prahl and A. J. Welch, "Light distributions in artery tissue: Monte Carlo simulations for finite-diameter laser beams," *Lasers in surgery and medicine,* vol. 9, no. 2, pp. 148-154, 1989.

[17] M. Keijzer, J. W. Pickering and M. J. van Gemert, "Laser beam diameter for port wine stain treatment," *Lasers in surgery and medicine,* vol. 11, no. 6, pp. 601-605, 1991.

[18] S. L. Jacques and L. Wang, "Monte Carlo modeling of light transport in tissues," in *Optical-Thermal Response of Laser-Irradiated Tissue*, Boston, MA, Springer US, 1995, pp. 73-100.

[19] L. Wang and S. L. Jacques, "Hybrid model of Monte Carlo simulation and diffusion theory for light reflectance by turbid media," *Journal of the Optical Society of America. A, Optics, image science, and vision,* vol. 10, no. 8, pp. 1746-1752, 1993.

[20] B. D. Chaurasia, Human anatomy vol. 1, India: CBS Publishers & Distributors Pvt Ltd, 1991.

[21] G. F. Odland, "Structure of skin," in *Physiology, Biochemistry and Molecular Biology of the skin*, New York, Oxford University Press, 1991, pp. 3-62.

[22] Q. Zhao, H. Kechang, A. Jianxiong and al, "The distance from skin to cervical and high thoracic epidural space on chinese adults as read from MRI," *Pain Physician,* vol. 17, no. 2, pp. 163-168, 2014.

[23] J. Mobley, "Optical Properties of Tissue," in *Biomedical Photonics Handbook*, T. Vo-Dinh, Ed., CRC Press, 2003.

[24] J. M. Schmitt, G. X. Zhou, E. C. Walker and R. T. Wall, "Multilayer model of photon diffusion in skin," *Journal of the Optical Society of America A,* vol. 7, no. 11, pp. 2141-2153, 1990.

[25] R. R. Anderson and J. A. Parrish, "The Optics of Human Skin," *Journal of Investigative Dermatology,* vol. 77, no. 1, pp. 13-19, 1981.